Thermocapillary-assisted pulling of contact-free liquid films

Benoit Scheid*
TIPs - Fluid Physics unit, Université Libre de Bruxelles C.P. 165/67, 1050 Brussels, Belgium, EU

Ernst A. van Nierop

Howard A. Stone
Department of Mechanical and Aerospace Engineering,
Princeton University, Princeton, NJ 08544, USA
(Dated: February 16, 2012)

We study the formation of a free liquid film that is pulled out of a bath at constant speed and stabilized by the action of thermocapillary stresses prescribed at the free surfaces. The basic concept was introduced recently (Applied Physics Letters **97**, 171906, 2010). The theory suggests that very thin ribbons of molten material can be drawn out of a melt by adequately tuning the temperature gradient along the dynamic meniscus that connects the static meniscus at the melting bath to the drawn flat film region. In the present paper, we extend our original analysis by investigating the roles of inertia and gravity on the film thickness, and show how the results depend on heat transfer/conduction properties. Furthermore, we analyze the one-dimensional transverse stability of the free film with respect to the long-wave thermocapillary instability.

I. INTRODUCTION

The push for renewable energy technologies has led to the desire, and associated challenges, to manufacture silicon films at high speed. One technique used in industry is the film-casting process [1], which consists of depositing the molten silicon through the bottom of a casting frame with a moving and sub-cooled substrate, so that a layer of the liquid metal crystallizes on the substrate and a silicon film is formed [2]. In this process, the molten silicon is in contact with a solid substrate, which can alter the quality of the ribbon. Alternatively, silicon sheets produced by vertical growth from a melt are contact-free, but production speeds are much smaller than in the aforementioned technique [3]: the speed for free-standing sheets is typically limited to a few cm/min to avoid breaking the liquid bridge between the melt and the foil. In fact, no stable film can be pulled out of a liquid bath if only extensional viscous and capillary forces are in balance [4]. Nevertheless, in the analogous process of pulling soap films from a liquid bath, large speeds (cm/s) can be attained due to shear stresses induced by surfactant concentration gradients at the free surfaces [5]. Surfactant can obviously not be used to produce foils of pure materials but interfacial thermocapillary stresses can be generated instead by prescribing temperature gradients along the free surfaces.

We recently reported on this concept of assisting the formation of free liquid films by thermocapillary stresses [6]. Though the ideas should be applicable to the production of contact-free foils at industrially competitive speeds, we focus here on the fluid dynamics aspects of this concept. First, we reiterate and expand on the problem formulation (§II) and discuss different distinguished limits of the dominant balances associated with the relevant stresses that act on the film (§III). We next go beyond the analysis presented before [6], addressing the roles of inertia and gravity (§IV), the influence of heat transfer and conduction (§V), and the possibility of a transverse thermocapillary instability (§VI). Understanding these themes is important for the control and practice of this processing idea.

II. PROBLEM FORMULATION

We consider a liquid film withdrawn with speed u_0 from a bath of temperature T_b as shown in Fig. 1. The film cools and solidifies at some distance above the bath. Symmetry is assumed about the x-axis. The far-field ambient temperature, denoted $T_a(x)$, is assumed to vary. The film thickness $h(x,t)$ is assumed to eventually approach a constant value h_0 at a distance sufficiently far above the bath and before it solidifies, as sketched in Fig. 1. The density ρ is taken to be constant [7][8] and the viscosity $\eta(T)$ depends on the temperature T. We denote the surface

*Electronic address: bscheid@ulb.ac.be

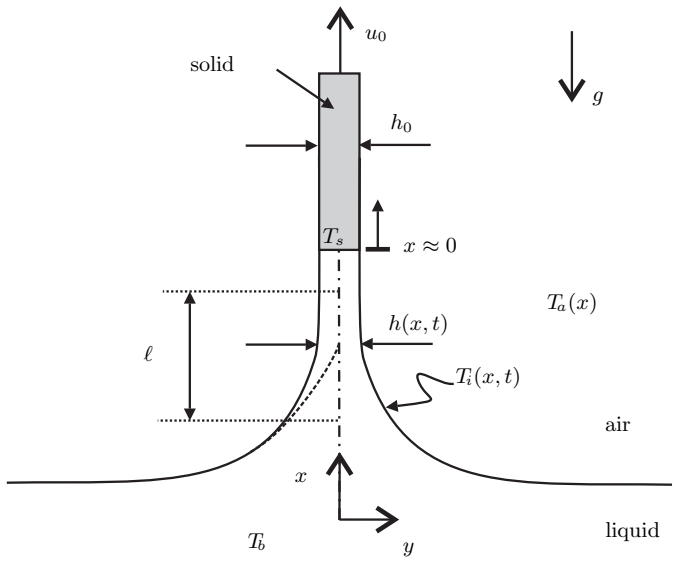

FIG. 1: Sketch of the film pulling problem for producing contact-free films. The dashed line indicates a static meniscus (not to scale). The film is pulled from a liquid bath and is assumed to solidify above $x = 0$ (gray shading).

temperature of the film as $T_i(x,t)$ and consider a linear decrease of the surface tension with temperature, which applies to most liquids including molten silicon,

$$\gamma(T_i) = \gamma_s - \gamma'(T_i - T_s) \ , \tag{1}$$

where $\gamma_s = \gamma(T_s)$, T_s is the solidification temperature, and $\gamma' = \left|\frac{\mathrm{d}\gamma}{\mathrm{d}T}\right|$ is a positive constant.

A. Mass conservation equation and stress balance

The mass conservation equation has the form

$$h_t + (h\bar{u})_x = 0 \ , \tag{2}$$

where $\bar{u}$ is the cross-sectionally averaged velocity, and the subscripts t and x indicate the time and space derivatives, respectively. For steady state, (2) reduces to

$$\bar{u}h = u_0 h_0 \ . \tag{3}$$

In the framework of lubrication theory, and following Breward [9], we can write a master equation including all possible sources of axial stresses in a film of pure liquid (see e.g. [4, 10]):

$$4\left(\bar{\eta}(\bar{T})h\bar{u}_x\right)_x - 2\gamma' T_{ix} + \frac{\gamma_s}{2} h h_{xxx} - \rho g h = \rho h(\bar{u}_t + \bar{u}\bar{u}_x) \ , \tag{4}$$

where $\bar{\eta}$ and $\bar{T}$ are the cross-sectionally averaged viscosity and temperature, respectively. The first term on the left-hand side in (4) represents the extensional viscous stress, where the factor 4 is the Trouton ratio. The second term accounts for thermocapillary stresses at both interfaces, the third term accounts for the stress induced by the gradient of the film curvature, and the fourth term represents stresses due to gravity. The right-hand side accounts for inertial effects.

B. One-dimensional temperature equation

We assume that the temperature distribution is one-dimensional, i.e.,

$$T(x,y,t) \equiv \bar{T}(x,t) = T_i(x,t) \ , \tag{5}$$

where $\bar{T}(x,t)$ is the cross-sectionally averaged temperature. This approximation is valid as a consequence of the thin-film asymptotic expansion, at least to first order, as outlined in Appendix B. The resulting energy equation is

$$\rho c_p h \left(\bar{T}_t + \bar{u}\bar{T}_x\right) = -2\alpha(\bar{T} - T_a) \,, \tag{6}$$

where c_p is the specific heat capacity and α is the effective heat transfer coefficient at the free surfaces due to both convective and radiative cooling. Even though the radiative heat transfer contribution is proportional to T^4, its linearized form is sufficient for the present problem as demonstrated in Appendix C. Consequently, $\alpha = \alpha_R + \alpha_C$, where α_R and α_C are, respectively, the radiative and convective heat transfer coefficients. The former is estimated in Appendix C, while the latter depends on the properties and the velocity of the surrounding gas. We assume here that forced convection removes at least as much energy as radiative transfer such that $\alpha \approx 10^3$ W/(m^{2}K) is taken for numerical examples that follow.

Heat conduction has been neglected here but will be treated later in §V B. We also neglect energy released during solidification because it is assumed to occur after the geometry is no longer changing [11]. In practical settings of course, this latent heat would need to be transported away from the film.

Finally, the viscosity is presumed to decrease linearly with temperature,

$$\bar{\eta}(\bar{T}) = \eta_s - \eta' \left(\bar{T} - T_s\right) \,, \tag{7}$$

where $\eta_s = \bar{\eta}(T_s)$ and $\eta' = \left|\frac{\mathrm{d}\eta}{\mathrm{d}T}\right|$ is a positive constant. This approximation is valid for small temperature changes, i.e. $|\bar{T} - T_s|/T_s \ll 1$.

C. Non-dimensionalization

We next nondimensionalize using the scalings

$$X = \frac{x}{\ell} \,, \quad H = \frac{h}{h_0} \,, \quad \bar{U} = \frac{\bar{u}}{u_0} \,, \quad \Upsilon = \frac{\bar{\eta}}{\eta_s} \,, \tag{8}$$

$$\bar{\Theta} = \frac{\bar{T} - T_s}{\Delta T} \,, \quad \Theta_a = \frac{T_a - T_s}{\Delta T} \,, \tag{9}$$

where ℓ is the characteristic length scale (to be determined) in the x-direction and $\Delta T = T_b - T_s$. As we are interested in steady pulling, we consider here stationary conditions, i.e. from (3),

$$\bar{U}H = 1 \,. \tag{10}$$

The stress balance (4) thus becomes

$$4\varepsilon^2\left(\Upsilon\frac{H_X}{H}\right)_X + 2\varepsilon Ma\bar{\Theta}_X - \frac{\varepsilon^3}{2Ca}HH_{XXX} + GH - \varepsilon Re\frac{H_X}{H^2} = 0 \,, \tag{11}$$

where $\varepsilon = h_0/\ell$ is the slenderness parameter, and the Marangoni, capillary, gravity and Reynolds numbers are, respectively,

$$Ma = \frac{\gamma'\Delta T}{\eta_s u_0}, \quad Ca = \frac{\eta_s u_0}{\gamma_s}, \quad G = \frac{\rho g h_0^2}{\eta_s u_0}, \quad Re = \frac{\rho h_0 u_0}{\eta_s} \,. \tag{12}$$

The asymptotic expansion leading to (11) is given in Appendix A. The dimensionless viscosity function has the form

$$\Upsilon(\bar{\Theta}) = 1 - \mu\bar{\Theta} \,, \tag{13}$$

where $\mu = \eta'\Delta T/\eta_s$ measures the sensitivity of the viscosity to temperature changes.

Likewise, the steady temperature equation (6) becomes

$$\bar{\Theta}_X = -St\left(\bar{\Theta} - \Theta_a(X)\right) \,. \tag{14}$$

The asymptotic expansion leading to (14) is given in Appendix A. The Stanton number, St, which measures the rate of energy transfered at both interfaces relative to the rate of energy advected by the main flow, is defined as

$$St = \frac{2\alpha\ell}{\rho c_p u_0 h_0} \equiv \frac{St'}{\varepsilon Ca} \quad \text{with} \quad St' = \frac{2\alpha}{\rho c_p(\gamma_s/\eta_s)} \,. \tag{15}$$

The parameter St' only depends on the fluid properties and on the heat transfer coefficient. Note that (14) is decoupled from the stress equation and can thus be solved independently provided that the ambient temperature $\Theta_a(x)$ is specified.

D. Controlled ambient temperature

To close the system of equations, we need to know the form of the ambient temperature $\Theta_a(x)$. We assume here that the function is prescribed and varies smoothly, in dimensionless form, from unity in the liquid bath to zero in the flat film region where the liquid solidifies. We can choose for instance a hyperbolic tangent function of the form

$$\Theta_a(X) = \frac{1}{2}\left(1 - \tanh\left\{\frac{2\pi}{D}\left(X + sD\right)\right\}\right) , \tag{16}$$

where $D = d/\ell$ is approximately the dimensionless distance over which the temperature difference ΔT is applied, with d the dimensional distance. We note that other functions such as an error function variation would lead to similar results as those that follow. Because the problem is invariant by translation, we have shifted the temperature variation by the quantity sD, with s the shift parameter. For $s = 1$, $\Theta_a(0) \approx 0$. In the following, the value of s has been fixed to ensure $\Theta(0) \approx 0$ such that $x = 0$ coincides approximately with the solidification front, i.e. $\bar{T} \approx T_s$. In practice, we have set $s = 1$ in the limit of infinite Stanton number (§IV) and $s = 6$ in the case of finite Stanton number (§V).

III. DOMAIN DECOMPOSITION

In the stationary regime, the film-pulling problem represented in Fig. 1 can be decomposed into three regions, each of which corresponds to a specific force balance: (A) a capillary static meniscus near the liquid bath where gravitational and capillary forces balance (third and fourth terms in (11)); (B) a flat film region of constant film thickness h_0; (C) a transition region between the (A) and (B), referred to as the "dynamic meniscus", in which, in principle, all forces can be in balance. An analogous decomposition relying on the slenderness assumption $\varepsilon \ll 1$ was used by Breward and Howell [12] to describe the drainage of a foam lamella. Next, we detail the specifics of each region:

(A) In the static meniscus region, the curvature can be calculated by balancing gravity and capillary forces. The curvature obtains a constant value, $h_{xx} = \sqrt{2}/\ell_c$, with $\ell_c = \sqrt{\gamma_0/(\rho g)}$ the capillary length (see [13] for instance), near the dynamic meniscus (C). This characterization is identical to the treatment of this region in the classical Landau-Levich-Derjaguin problem [14, 15].

(B) As mentioned above, the geometry is assumed to no longer change beyond the dynamic meniscus, and up to the solidification front. Relaxing this assumption would require also solving for the film thickness in this region. In such a case, there will be a balance between at least the three first terms in (11), with a plug flow velocity profile (to leading order). The flow in this region would indeed be primarily extensional, with a decrease of the film thickness along the x-direction until the solidification front. According to [12] this extensional flow regime corresponds to the distinguished limit of the master equation (11) where $Ma = O(\varepsilon)$ and $Ca = O(\varepsilon)$. Nevertheless, we will show that in the limit of large Marangoni stresses as in region (C), the effect of extensional viscous stress can be neglected, and the film thickness can be assumed effectively constant, as considered below.

(C) As pointed out in [4] no free film can be stably pulled out of a liquid bath in the extensional flow limit. In order to pull a film, sufficiently large shear stress should be present at the free surface, as is assumed to be the case here. The flow is therefore shear-driven in this region, and has a parabolic velocity profile across the film. Consequently, capillary and Marangoni effects primarily balance and the extensional viscous stress is negligible. Again, according to [12], this shear flow regime corresponds to the distinguished limit of the master equation (11) where $Ma = O(\varepsilon^{-1})$ and $Ca = O(\varepsilon^3)$. This limit thus requires the Marangoni number to be much larger than unity.

Based on this domain decomposition, the film thickness profile in the transition region (C) must match with the curvature of the static meniscus (A) as the film thickens, namely $H_{XX} = \sqrt{2}\ell^2/(\ell_c h_0)$ as $X \to -\infty$. Therefore, the matching condition allows the determination of h_0:

$$\frac{h_0}{\ell_c} = \frac{H_{XX}}{\sqrt{2}}\varepsilon^2 \quad \text{as} \quad X \to -\infty , \tag{17}$$

where $H_{XX}(-\infty)$ remains to be determined. Also, $\varepsilon = h_0/\ell$ needs to be explicitly given, which will appear to be independent of h_0, i.e. for $\ell \propto h_0$.

TABLE I: Set of parameters for silicon. The physical properties are given at the melting temperature $T_s = 1687\,\mathrm{K}$ [7].

Properties:	density	ρ	$\mathrm{kg/m^3}$	2583
	dynamic viscosity	η_s	Pa.s	5.57×10^{-4}
	viscosity variation	η'	Pa.s/K	5.39×10^{-7}
	surface tension	γ_s	N/m	0.721
	surface tension variation	γ'	N/(m K)	6×10^{-5}
	heat capacity	c_p	J/(kg K)	910
	thermal conductivity	κ	W/(m K)	22.1
	gravitational acceleration	g	$\mathrm{m/s^2}$	9.81
	capillary length	ℓ_c	m	5.3×10^{-3}
Control parameters:	pulling velocity	u_0	m/s	10^{-2}
	temperature difference	ΔT	K	10^2
	length of T variation	d	m	10^{-3}
	heat transfer coefficient	α	$\mathrm{W/(m^2\,K)}$	10^3
Output parameters:	film thickness	h_0	m	10^{-4}
	dynamic length	ℓ	m	10^{-3}
Dimensionless numbers:	capillary number	Ca	$\eta_s u_0/\gamma_s$	10^{-5}
	Marangoni number	Ma	$\gamma'\Delta T/(\eta_s u_0)$	10^3
	aspect ratio	ε	h_0/ℓ	10^{-1}
	gravity number	G	$\rho g h_0^2/(\eta_s u_0)$	10
	Reynolds number	Re	$\rho h_0 u_0/\eta_s$	1
	Péclèt number	Pe	$\rho c_p u_0 h_0/\kappa$	10^{-1}
	Biot number	Bi	$\alpha h_0/\kappa$	10^{-1}
	Stanton number	St	$2\alpha\ell/(\rho c_p u_0 h_0)$	1
	alternate Stanton number	St'	$2\alpha\eta_s/(\rho c_p \gamma_s)$	10^{-6}
	Weber number	We	$\rho \ell_c u_0^2/\gamma_s$	10^{-3}
	Surface tension variation	Γ	$\gamma'\Delta T/\gamma_s$	10^{-2}
	Viscosity variation	μ	$\eta'\Delta T/\eta_s$	10^{-1}

Furthermore, the film thickness equation (11), with only the relevant terms, should be solved in the transition region (C) with the boundary conditions:

$$H \to 1\,, \quad H_X \to 0\,, \quad H_{XX} \to 0 \quad \text{as} \quad X \to \infty, \tag{18}$$

i.e. approaching the flat film region (B) above the bath. This condition is mathematically rigorous as far as the film remains liquid. In case of a solidification front somewhere in the film region (B), the bound for (18) should rather be finite for consistency. In any case, the numerical solution for H should be sought in a finite domain, $X \in [-L_1, L_2]$, such that the boundary conditions (18) and the matching condition (17) are replaced by $H(L_2) = 1$, $H_X(L_2) = 0$, $H_{XX}(L_2) = 0$ and $H_{XX}(-L_1) = \sqrt{2}\ell^2/(\ell_c h_0)$. As mentioned, a steady flat film can only exist through the presence of thermocapillary stresses at the interfaces induced by the imposed temperature gradient. Therefore, the position of the dynamic meniscus should be obtained relative to the position of the imposed temperature distribution $\Theta_a(X)$. The origin $X = 0$ can thus be anywhere between $+\infty$ and $-\infty$ or, for the numerical solution, between $-L_1$ and L_2. Now, the hyperbolic tangent function chosen for the temperature distribution quickly approaches the solidification temperature as X tends to $+\infty$, in fact over a length of about D. Therefore translating Θ_a by the distance sD, with $s \geq 1$ ensures $\Theta(0) \approx 0$, and allows us to set $L_2 = 0$, which simplifies the subsequent developments. For the value of L_1, we simply choose it to be large enough in numerical computations to ensure that $H_{XX} \to$ constant as $X \to L_1$ so that $H_{XX}(-L_1) = H_{XX}(-\infty)$ within the numerical accuracy.

IV. PARAMETRIC STUDY

Based on the physical properties of silicon and on the control parameters, we assess the values of the dimensionless numbers in Table I. The value of ε has been assessed by assuming the length of the dynamic meniscus is much smaller than the length of the static meniscus, i.e. $\ell \ll \ell_c$. Since the lubrication approximation also implies that $\ell \gg h_0$, a first estimate of ℓ can simply be the geometric mean $\ell = \sqrt{h_0 \ell_c}$, such that $\varepsilon = O(\sqrt{h_0/\ell_c})$, which inserted into (17) makes $H_{XX}(-\infty) = O(1)$ as expected. For films of about $100\,\mu$m, which is typically the order of magnitude in many industrial processes we are interested in, $\varepsilon = O(10^{-1})$. From Table I, we then get $Ma \geq O(\varepsilon^{-1})$ and $Ca \leq O(\varepsilon^3)$, which matches the conditions for the "shear" distinguished limit of the thin film stress equation for which the extensional

viscous effects can be safely neglected. Moreover, we find in Table I that $\mu = O(\varepsilon)$, and the assumed dependence of the viscosity with temperature (13) ensures that Υ remains of the order of unity. These estimates are reasonable at least for liquids with viscosities that do not diverge when approaching the solidification temperature, as is the case for silicon [16].

Now, as in our previous work [6], we construct the length scale ℓ in the x-direction for the dynamic meniscus from the dominant balance between surface tension and Marangoni effects. This step yields

$$\varepsilon^2 = 4\Gamma \qquad \text{or} \qquad \ell = \frac{h_0}{2\sqrt{\Gamma}}\,, \tag{19a}$$

$$\text{where} \quad \Gamma \equiv CaMa = \frac{\gamma' \Delta T}{\gamma_0}\,, \tag{19b}$$

which measures the relative change of surface tension with temperature. Multiplying (11) by $2Ca/\varepsilon^3$ and using (19a) leads to

$$\zeta \left(\frac{H_X}{H}\right)_X + \bar{\Theta}_X - HH_{XXX} + \beta H - \delta \frac{H_X}{H^2} = 0\,, \tag{20}$$

where

$$\zeta = \frac{4Ca}{\sqrt{\Gamma}}\,, \quad \beta = \frac{1}{4\Gamma^{3/2}} \frac{h_0^2}{\ell_c^2} \quad \text{and} \quad \delta = \frac{We}{2\Gamma} \frac{h_0}{\ell_c}\,, \tag{21}$$

with $We = \rho \ell_c u_0^2/\gamma_s$ the Weber number. According to Table I, using $h_0 \approx 100\,\mu$m, we get $\zeta = O(10^{-4})$, $\beta = O(10^{-1})$ and $\delta = O(10^{-2})$ such that viscous, gravity and inertia terms remain small as compared to capillary and Marangoni terms in (20), as assumed initially. Nevertheless, because We varies with the square of the pulling speed, for the parameters in Table I a pulling speed of a few tenths of centimeters per second would make $\delta = O(1)$, which thus requires including inertia in the calculation. An increase of the film thickness would also make gravity significant. The roles of inertia and gravity are thus addressed hereafter.

A. Role of inertia

Integrating (20) without viscous and gravity terms, i.e. $\zeta = \beta = 0$, using $H \to 1$, $H_X \to 0$, $H_{XX} \to 0$ and $\Theta \to 0$ as $X \to \infty$, we obtain

$$HH_{XX} - \frac{1}{2} H_X^2 + \delta \left(1 - \frac{1}{H}\right) = \bar{\Theta}\,. \tag{22}$$

This equation should be coupled to the heat equation (14), which we initially simplify in the limit of large Stanton numbers. Indeed, in the case $St \gg 1$, Scheid *et al.* [17] have shown that $\bar{\Theta} \approx \Theta_a$, which correspond to a "prescribed temperature" limit. In such a case, Eq. (22), using (16), becomes

$$2HH_{XX} - H_X^2 + 2\delta \left(1 - \frac{1}{H}\right) = 1 - \tanh\left\{2\pi \left(\frac{X}{D} + 1\right)\right\}\,. \tag{23}$$

Note that for the typical parameters in Table I, a large Stanton number of $St = 10$ for instance would correspond to an effective heat transfer coefficient of $\alpha \approx 10000$ W/(m^{2}K), which is technologically challenging. Therefore, the more realistic case of $St = O(1)$ is treated separately later in §V.

Solving (23) numerically with the boundary conditions $H(0) = 1$ and $H_X(0) = 0$, the curvature of the thickness profile tends to a constant as $X \to -\infty$. The value of $H_{XX}(-\infty)$ versus D is reported in Fig. 2 with and without inertial effects, i.e. for $\delta = 1$ and 0. Using the value of $H_{XX}(-\infty)$ in (17) finally allows determination of the film thickness of a thermocapillary-assisted contact-free film.

1. *Strong temperature gradient: $D \lesssim 1$ or $d \lesssim \ell$*

We observe in Fig. 2 that $H_{XX}(-\infty)$ tends to a constant value as $D \to 0$, and even for $D \lesssim 1$. Contrary to the case with no inertia, i.e. $\delta = 0$, for which $H_{XX}(-\infty)$ tends to unity (dotted line), we have not been able to determine, like in [6], an analytical solution for $H_{XX}(-\infty)$ in the limit of $D \to 0$. Nevertheless, we numerically obtain the relation

$$H_{XX}(-\infty) \approx 1 - \frac{\delta}{2} \quad \text{for} \quad D \lesssim 1\,. \tag{24}$$

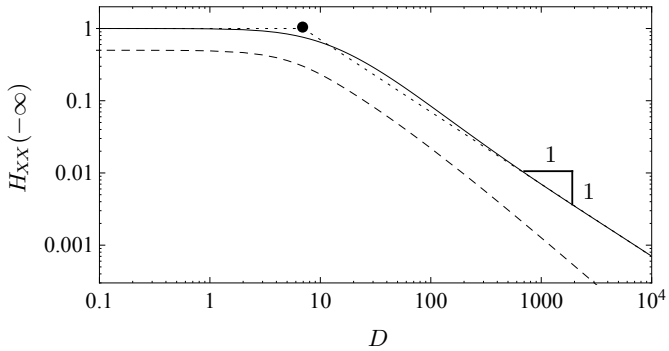

FIG. 2: Matching curvature $H_{XX}(-\infty)$ versus the dimensionless length D over which the temperature varies along the X-direction: solid line corresponds to no inertia, $\delta = 0$; dashed line corresponds to finite inertia, $\delta = 1$. The dotted lines correspond to the asymptotes for $D \to 0$ and $D \to \infty$, and the black dot indicates the crossover (see text for details).

Obviously, (24) requires $\delta < 2$ for the film thickness to be finite. Combining (17) with (24), and using (21), leads to

$$h_0 \approx 2\sqrt{2}\,\ell_c\,\Gamma\left(1+\frac{We}{\sqrt{2}}\right)^{-1} \quad \text{for} \quad D \lesssim 1\,. \tag{25}$$

This result shows that the thickness is proportional to the amplitude of the surface tension change along the interface, but does not depend on the distance d along which this change occurs, provided this distance remains shorter than or equal to the characteristic length of the dynamic meniscus ℓ. Additionally, the thickness decreases as the Weber number, or equivalently as the pulling speed, increases.

As an example, consider producing a silicon film of 100 μm thick at a pulling speed of 10 cm/s, which would require a value of $\Gamma = 0.008$, or a variation of surface tension of 5 mN/m over at most the length $\ell \approx (\sqrt{2} - We)\ell_c\sqrt{\Gamma}$ (i.e. $D \lesssim 1$). This feature requires lowering the temperature of the surface of the film by about 100 K over a distance smaller than or equal to 1 mm. We observe here that the estimate is very similar for a pulling speed of 10 cm/s as for 1 cm/s and this is true as long as $We \ll 1$. In the limit of $We = 0$, we recover our previous result reported in [6] for which the thickness was independent of the pulling speed.

2. *Weak temperature gradient: $D \gg 1$ or $d \gg \ell$*

We observe in Fig. 2 (dotted line) that $H_{XX}(-\infty)$ scales like D^{-1} as $D \to \infty$, at least for $\delta = 0$. This behavior suggests that, in the limit corresponding to a weak temperature gradient, another scaling than (25) applies for the film thickness. The dotted line in Fig. 2 corresponds to $7/D$, which we shall take to approximate $H_{XX}(-\infty)$ when $D \gg 1$. In such a case, the matching condition (17) becomes $h_0 \approx 2\sqrt{2}\ell_c\Gamma(7/D)$. Substituting $D = d/\ell$ and eliminating ℓ by taking the original length-scale for the dynamic meniscus $\ell = \sqrt{h_0\ell_c}$ (indeed, the length-scale (19a) does not hold in this regime), we obtain

$$h_0 \approx 392\,\ell_c^3\frac{\Gamma^2}{d^2} \quad \text{for} \quad D \gg 1\,. \tag{26}$$

This result shows that the thickness is proportional to the square of the temperature gradient $\Delta T/d$. An identical scaling law has been obtained by Carles, Cazabat and coworker [18, 19] for the problem of a liquid film climbing up a vertical plate driven by a temperature gradient . The scaling law (26) could also have been obtained from Eq. (4), apart for the prefactor, by balancing the Marangoni and the surface tension terms as follow:

$$\gamma'\frac{\Delta T}{d} \sim \gamma_s\frac{h_0^2}{\ell^3} \quad \text{for} \quad d \gg \ell\,, \tag{27}$$

and eliminating $\ell = \sqrt{h_0\ell_c}$. Also, the scaling law for the case of a strong temperature gradient is recovered by replacing d by ℓ in (27), which gives $h_0 \sim \ell_c\Gamma$, as found in (25) for $We = 0$.

In the case of $\delta = 1$, we observe in Fig. 2 (dashed line) that $H_{XX}(-\infty)$ scales like D^{-n} as $D \to \infty$, with $n > 1$, indicating again in this regime that for a given temperature, the thickness will be smaller with inertia than without it, and increasingly so for large D. However, the correction is weak in any event.

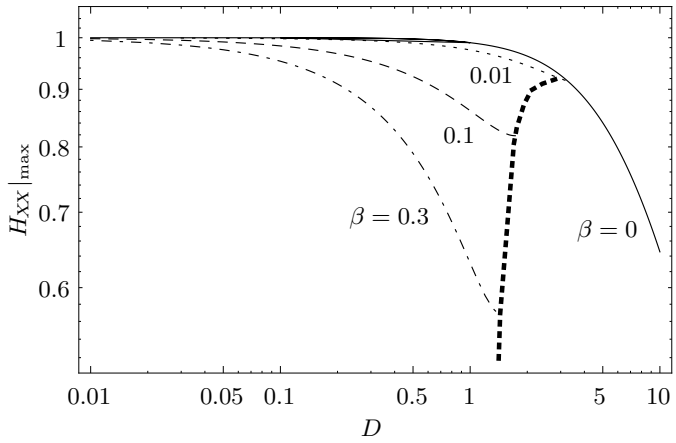

FIG. 3: Matching curvature $H_{XX}|_{\max}$ versus the dimensionless length D for various β, solving (20) with $\zeta = \delta = 0$. The curve for $\beta = 0$ has been matched with $H_{XX}(-\infty)$ as previously. The thick dashed line is the loci of the minimum of $H_{XX}|_{\max}$ corresponding to the "drainage limit".

As an example, taking again $\Gamma \approx 10^{-2}$, but imposing the temperature difference over a length $d = 1$ cm, the film thickness estimated with (26) is now about 10 μm. If the length is further increased to $d = 10$ cm, the film thickness reaches 100 nm, which is known to be critical for rupture due to van der Waals forces. It seems there is thus a minimum temperature gradient below which no film can be formed, which is typically of about 1 K/mm for silicon film. In reality, the temperature gradient should be much larger than that value to counterbalance the effect of gravitational drainage as shown next in §IV B.

3. *Crossover between the two above regimes*

The crossover between the two regimes described above, and indicated by a black dot in Fig. 2 for the case with no inertia, is obtained by equating (25) with $We = 0$ and (26). The result is

$$d^* \approx 12\ell_c\sqrt{\Gamma}\,. \tag{28}$$

Consequently, if $d \ll d^*$, the scaling law for the thickness is (25) and if $d \gg d^*$, the scaling law is (26).

B. Role of gravity

We now examine the influence of gravity, i.e. for $\beta \neq 0$, by considering the stress balance (20) without extensional viscous and inertial effects, i.e. $\zeta = \delta = 0$. As obtained from our numerical results (not shown), the solutions do not tend to a constant curvature as $X \to -\infty$, as was the case for $\beta = 0$. Instead, as $X \to -\infty$ the curvature passes through a maximum before decreasing and eventually becoming negative. Following the work by de Ryck and Quéré [20] on plate coating, we match the static and the dynamic menisci using the maximum curvature, denoted by $H_{XX}|_{\max}$ hereafter. This choice for the matching curvature possibly overestimates the film thickness but has the advantage that it recovers the same curvature as the one obtained in the absence of gravity for $\beta \to 0$. The corresponding film thickness then follows from (17) once H_{XX} is specified.

For various values of the gravitational parameter β, we report in Fig. 3 the maximum curvature $H_{XX}|_{\max}$ versus the length D, which controls the temperature gradient along the interface. We find that as D increases, the maximum curvature $H_{XX}|_{\max}$ passes through a minimum before diverging. In Fig. 3, we only plotted the curves before that curvature minimum, and we plot the loci of the minima as represented by the thick dotted line. Indeed, since the thickness can only decrease due to gravity when the strength of the temperature gradient is reduced, we conclude that the divergence of $H_{XX}|_{\max}$ (not shown) is unphysical and is the signature that the Marangoni stresses become too weak to counterbalance gravitational drainage. The thick dotted line thus corresponds to the "drainage limit" beyond which no stable film can be formed. The fact that this "drainage limit" intersects with the curve obtained in the absence of gravity is because the two curves are constructed with two different matching curvatures (see §IV C). Nevertheless, this intersection occurs for $\beta \lesssim 0.01$, i.e. for regimes where gravity can safely be neglected.

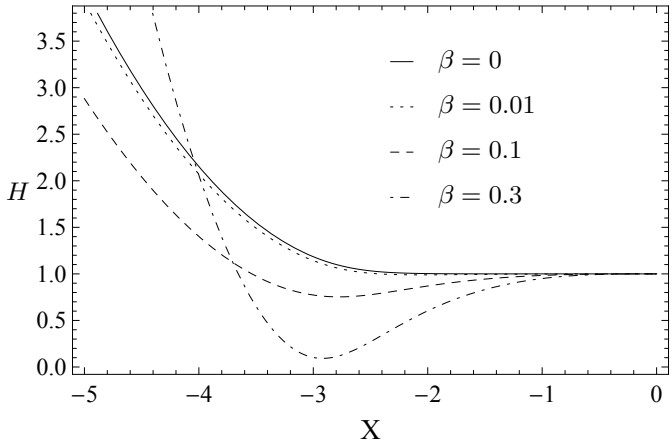

FIG. 4: Thickness profiles for $D = 2.5$ and various β, solving (20) with $\zeta = \delta = 0$.

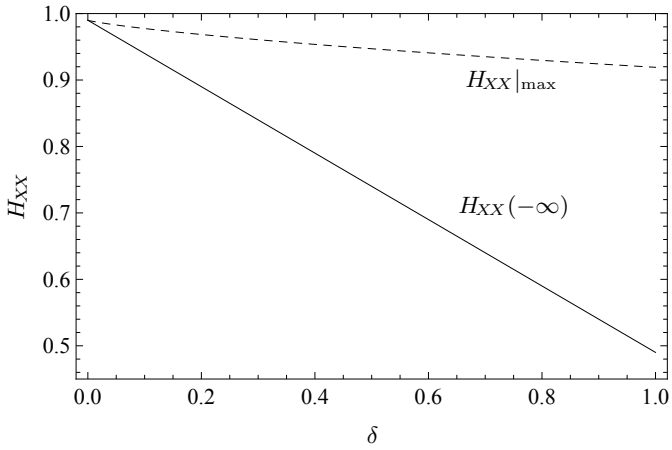

FIG. 5: Two different matching curvatures versus the inertia parameter δ with $\zeta = \beta = 0$ and $D = 1$.

To illustrate the limitation due to drainage, we plot in Fig. 4 the thickness profile for various β and at a fixed value of the parameter $D = 2.5$. The profiles for $\beta = 0.1$ and 0.3 show a minimum as a consequence of the drainage. Indeed, conditions are such that they lie beyond the "drainage limit" as depicted in Fig. 3, and should thus be avoided.

Analyzing the influence of gravity shows that the distance D — or alternatively the imposed temperature gradient — should be small enough to sustain a free film that is not overcome by gravitational drainage. Based on results in Fig. 3 as well as on the estimate $\beta = O(10^{-1})$, if the temperature gradient is imposed on a length equal to the length of the dynamic meniscus (i.e. $D \approx 1$), the film thickness would be about 15% smaller than the thickness predicted by (25) with $We = 0$ due to the sole action of gravity.

C. Coupling between gravity and inertia effects

In §IV A, we investigated the sole influence of inertia using $H_{XX}(-\infty)$ in the matching condition (17) while in §IV B we investigated the influence of gravity only using $H_{XX}|_{\max}$ as the matching curvature, since the curvature never reaches a constant value in this latter case. In fact, when considering inertial effects only, the curvature calculated from (20) with $\beta = \zeta = 0$ passes also through a maximum $H_{XX}|_{\max}$ as X is decreased before reaching a constant value $H_{XX}(-\infty)$ as $X \to -\infty$. Now that we want to analyze the influence of both inertia and gravity together, we should first assess for inertial effects only the consequences of using $H_{XX}|_{\max}$ instead of $H_{XX}(-\infty)$ as a matching condition. Fig. 5 shows both possible matching curvatures as a function of the inertia parameter δ. We see that as δ increases, $H_{XX}|_{\max}$ decreases much less than $H_{XX}(-\infty)$. Consequently, using $H_{XX}|_{\max}$ instead of $H_{XX}(-\infty)$ in

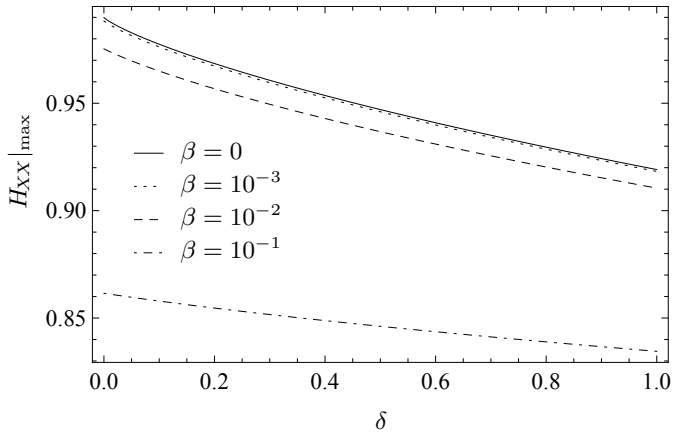

FIG. 6: Matching curvature $H_{XX}|_{\max}$ for various gravitational parameters β with $\zeta = 0$ and $D = 1$.

the matching condition (17) will overestimate the film thickness h_0, as already anticipated. However, for reasonable values of $\delta = O(10^{-1})$, the difference between both results is about 5% or less for $\delta \lesssim 0.1$ but increases rapidly for $\delta > 0.1$. In such a case, using $H_{XX}(-\infty)$ as a matching curvature is a more conservative approach as it gives smaller values of the film thickness than with $H_{XX}|_{\max}$.

Next, we evaluate the effect of both inertia and gravity using $H_{XX}|_{\max}$ since the curvature does not reach a constant value as $X \to -\infty$. Results are shown in Fig. 6. For reasonable values $\delta = O(10^{-1})$ and $\beta = O(10^{-1})$ (based on parameter values in Table I), the film thickness will be about 10% smaller than the thickness predicted by (25), which shows that this latter equation provides a good estimate of the film thickness as long as $\delta \lesssim 0.1$ and $\beta \lesssim 0.1$.

V. FINITE HEAT TRANSFER PHENOMENA

A. Influence of finite Stanton numbers

In this section, we relax the prescribed temperature assumption for infinite heat transfer coefficients, i.e. $\bar{\Theta} = \Theta_a(X)$, and solve the steady temperature equation (14) for finite Stanton numbers. The solution is expressed in terms of an hypergeometric function:

$$\bar{\Theta}(X) = {}_2F_1\left[1, \frac{StD}{4\pi}; 1 + \frac{StD}{4\pi}; -e^{\frac{4\pi(X+D)}{D}}\right] , \tag{29}$$

where the integration constant has been set to zero to avoid the divergence of the solution as $X \to -\infty$, ensuring that $\bar{\Theta}(-\infty) = 1$. Figure 7 shows the dependence of the temperature distribution in the film with the Stanton number. We see that decreasing the Stanton number, i.e. decreasing the heat transfer coefficient, has the effect of increasing the effective length, say D_{eff}, over which the temperature decreases from 1 to 0 in the x direction. It thus weakens the thermocapillary stresses at the free surfaces. Note also that the Stanton number decreases with increasing pulling speed, again reducing the effective temperature gradient.

The important feature here is that solving the temperature equation for finite St does not change qualitatively the results obtained in the limit of $St \to \infty$. For example, in the case of silicon, $St \approx 10$ for a pulling speed of 1 mm/s and a heat transfer coefficient of 1000 W/(m^{2}K), which gives a very small deviation from the limit of $St \to \infty$, as shown in Fig. 7. Now, increasing the puling speed to 1 cm/s gives $St = 1$ and thus, from Fig. 7, an effective temperature gradient which is about 3 times smaller than for $St = 10$. However, this negative effect could be compensated by decreasing the ambient temperature to temperature much lower than the melting temperature, i.e. $\min(T_a) \ll T_s$, but this analysis is beyond the scope of the present paper (see also the Conclusions).

B. Role of heat conduction

As a consequence of considering finite St, we should also investigate the influence of heat conduction in the liquid along the flow direction, as to some extent both effects, heat exchange with the surrounding and heat conduction along

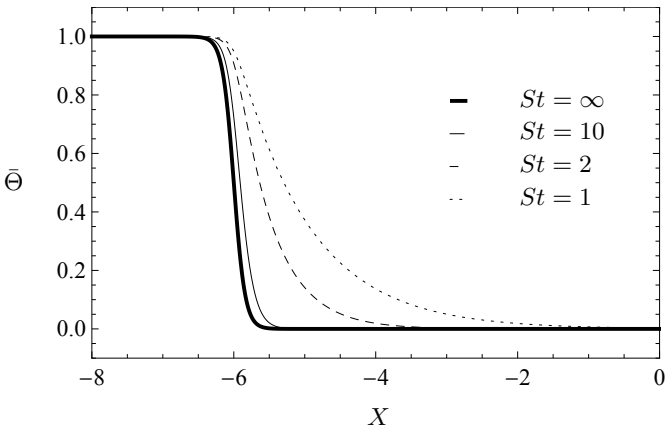

FIG. 7: Temperature distribution for various values of the Stanton number St, with $D = 1$ and $s = 6$.

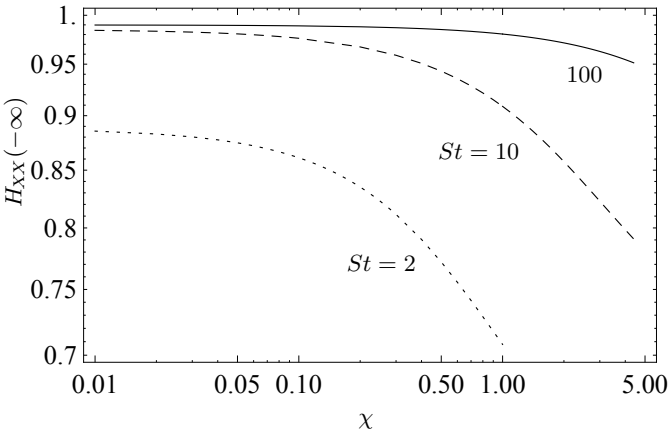

FIG. 8: Matching curvature versus the heat conduction parameter χ for various values of the Stanton number St. The results are obtained numerically with $\zeta = \delta = \beta = 0$ and $D = 1$.

the film, might become of the same order of magnitude. Therefore, we rewrite the averaged temperature equation including a conduction term (see details in Appendix B 3):

$$\bar{\Theta}_X = -St\left(\bar{\Theta} - \Theta_a\right) + \chi H \bar{\Theta}_{XX}\,, \tag{30}$$

where $\chi = \varepsilon/Pe$ is the effective heat conduction parameter that results from the scaling. According to Table I, $\chi = O(1)$, which indicates that longitudinal heat conduction can have a non-negligible influence, though is essentially limited to small speeds, namely for $Pe \lesssim \varepsilon$, which corresponds to $u_0 \lesssim 1\,\mathrm{cm/s}$ in the example of silicon. Since (30) now depends on the film thickness H, this equation should be solved together with (20) and the corresponding boundary conditions. We used the software COMSOL to compute solutions with the shift parameter set to $s = 6$, ensuring $\bar{\Theta}(0) \approx 0$ for all solutions (see §II D).

The matching curvature versus the heat conduction parameter χ is plotted in Fig. 8 for various Stanton numbers and a fixed value of $D = 1$. Inertia and gravitational effects have been neglected for the sake of clarity. As should be expected, increasing heat conduction decreases the effective temperature gradient and therefore reduces the matching curvature, hence the film thickness. This effect becomes negligible as $St \to \infty$ but can be significant for $St = O(1)$.

VI. TRANSVERSE MARANGONI INSTABILITY OF A UNIFORM FILM

We are also interested in analyzing the transverse stability of the stationary solutions $h(x)$ and $\bar{T}(x)$ found above. However, the fact that the base state depends on the x-coordinate makes the analysis more complex as it implies the

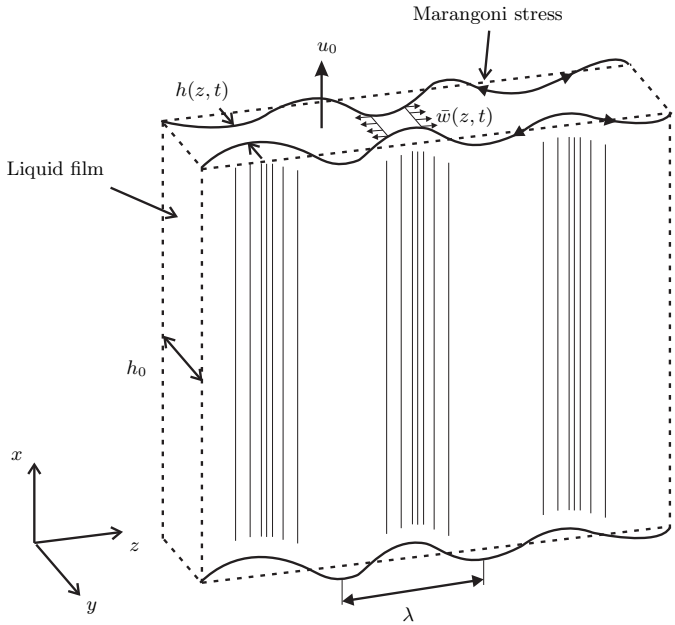

FIG. 9: Transverse modulations $h(z,t)$ of a uniform film of thickness h_0 due to the long-wave Marangoni instability; λ is the most amplified wavelength, $\bar{w}(z,t)$ is the thickness-averaged transverse velocity and u_0 is the uniform velocity in the x direction.

resolution of an eigenvalue problem with complex eigenvectors that also depend on the x-coordinate. Here we simplify the stability analysis by considering one-dimensional transverse modulations of the pulling film at a given position of the film profile $h(x_0) = h_0$. This case is equivalent to the transverse stability analysis of a two-dimensional uniform film of thickness h_0 as sketched in Fig. 9. Now, because h_0 is a parameter of the stability analysis, changing its value corresponds to changing the position along the profile $h(x)$. Of course this approach is simplistic as it does not account for convection of the perturbations in the x-direction. However, our analysis provides relevant information about the instability mechanism and typical wavelengths. The complete stability analysis of x-dependent base states is a subject for future work.

A. Mechanism and problem set-up

Here, we consider the stability of a two-dimensional unbounded film of mean thickness h_0 as illustrated in Fig. 9. We denote z the transverse coordinate, t the time, $\bar{w}(z,t)$ the thickness-averaged transverse velocity, and we neglect any variations with x. Considering the unsteady case, the conservation equation for the film thickness $h(z,t)$ takes the form

$$h_t + (h\bar{w})_z = 0 \,, \tag{31}$$

while the stress balance equation is similar to (4) with gravitational effects neglected:

$$4\eta\left(h\bar{w}_z\right)_z - 2\gamma' T_{iz} + \frac{\gamma_s}{2} h h_{zzz} - \rho h\left(\bar{w}_t + \bar{w}\bar{w}_z\right) = 0 \,. \tag{32}$$

As for the x direction, we shall scale z by ℓ. Also, since the transverse component of the velocity can only exist through perturbations of the main flow, we shall scale w by a small quantity εu_0. The scaling for the new variables is therefore

$$Z = \frac{z}{\ell}\,, \quad \bar{W} = \frac{\bar{w}}{\varepsilon u_0}\,, \quad \tau = \frac{\ell}{\varepsilon u_0} t\,, \quad \text{and} \quad H = \frac{h}{h_0}\,.$$

The dimensionless conservation and transverse stress-balance equations become

$$H_\tau + (H\bar{W})_Z \;=\; 0 \,, \tag{33a}$$

$$2We_\perp H(\bar{W}_\tau + \bar{W}\bar{W}_Z) = HH_{ZZZ} - \Theta_{iZ} + 8Ca(H\bar{W}_Z)_Z \ , \tag{33b}$$

where $We_\perp \equiv \varepsilon^2\delta/2 = (h_0/\ell_c)We$.

Equation (33b) needs to be complemented by an equation for the interfacial temperature Θ_i. Since we are considering the case of a uniform film, the heat can only be transferred through the interfaces, which is not compatible with a uniform temperature distribution across the film as considered so far. We are thus restricted here to the large heat transfer limit as treated in Appendix B 2 for which the temperature profile across the film has been assumed parabolic. Equation (B8) thus provides

$$\Theta_i = \frac{\bar{\Theta} + \frac{Bi}{6}H\Theta_a}{1 + \frac{Bi}{6}H} \ , \tag{34}$$

such that the surface temperature now depends on the film thickness. This dependence is reminiscent of the long-wave Marangoni instability whose mechanism is described below. Note that this dependence was not included in calculating solutions in the previous sections since we only considered stationary conditions. However, the Marangoni instability in the longitudinal direction would not have been relevant provided the temperature gradient across the layer, denoted $\Delta T_\perp/h_0$ with $\Delta T_\perp$ the perpendicular temperature difference, i.e. along the y-direction, remains much smaller than the temperature gradient imposed by the non-uniform ambient temperature, i.e. $\Delta T/\ell$. The corresponding condition for neglecting the Marangoni instability in the longitudinal direction is therefore $\Delta T_\perp/\Delta T \ll \varepsilon$.

As we consider the stability of a film of uniform thickness, the thickness-averaged temperature should also be uniform. Let us thus set $\bar{\Theta} = 1$ and $\Theta_a = 0$, such that the only parameter that accounts for the temperature constraint is the temperature difference $\Delta T_\perp$ between the mean temperature of the film and the temperature of the ambient. The interfacial temperature then becomes

$$\Theta_i = \frac{1}{1 + \frac{Bi}{6}H} \ , \tag{35}$$

which only depends on the thickness $H(Z,\tau)$ and provides the instability mechanism for the long-wave thermocapillary (Marangoni) instability: a perturbation leading to a thickening (respectively, thinning) of the film will induce a decrease (respectively, increase) of the interfacial temperature, hence an increase (respectively, decrease) of the surface tension.

B. Wavelengths and growth rates

Assuming normal mode perturbations of the uniform film, we write

$$H(Z,\tau) = 1 + a\, e^{ikZ+\sigma\tau} \ , \tag{36a}$$

$$W(Z,\tau) = b\, e^{ikZ+\sigma\tau} \ , \tag{36b}$$

where $a, b \ll 1$ are small amplitudes, $i = \sqrt{-1}$, k is the dimensionless wavenumber and σ is the dimensionless growth rate. Inserting these perturbations (36) into (33) using (35) and linearizing with respect to a and b, leads to the dispersion relation

$$\sigma = \frac{k}{2We_\perp}\left(\sqrt{2We_\perp\,(k_c^2 - k^2) + 16Ca^2k^2} - 4Cak\right) \ , \tag{37}$$

where the cut-off wavenumber for which σ vanishes in a nontrivial way is

$$k_c = \frac{\sqrt{6Bi}}{6 + 6Bi} \ . \tag{38}$$

The film is therefore unstable for $\sigma > 0$, i.e. for $0 < k < k_c$. We can then write the growth rate and the wavenumber of the most unstable mode:

$$\sigma_M = \frac{k_c^2}{8Ca + 2\sqrt{2We_\perp}} \ , \tag{39}$$

$$k_M = \frac{k_c}{\sqrt{2 + \frac{8Ca}{\sqrt{2We_\perp}}}} \ . \tag{40}$$

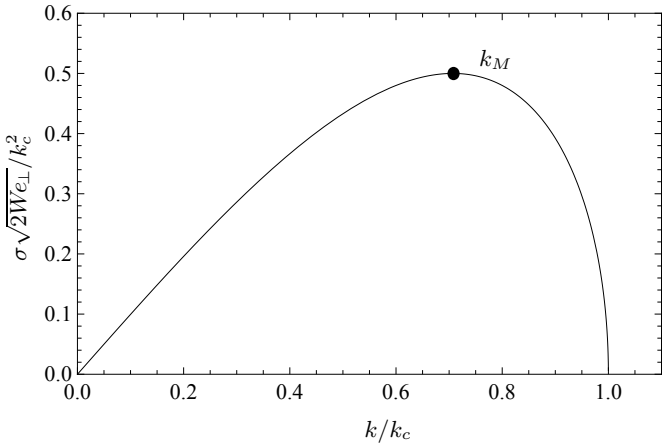

FIG. 10: Universal dispersion curve from (41). The black dot represents the most amplified modes corresponding to k_M and σ_M.

From Table I, we find that $8Ca/\sqrt{2We_\perp} \ll 1$, such that in the large surface tension limit ($Ca \to 0$), we obtain the simplified forms

$$\sigma = k\sqrt{\frac{k_c^2 - k^2}{2We_\perp}} , \tag{41}$$

$$\sigma_M = \frac{k_c^2}{2\sqrt{2We_\perp}} , \tag{42}$$

$$k_M = \frac{k_c}{\sqrt{2}} . \tag{43}$$

A universal dispersion curve is drawn in Fig. 10. We can observe that increasing the critical wavenumber, or equivalently the Biot number, enhances the instability: it not only increases the growth rate of the instability but also the range of unstable wavenumbers. In dimensional form, we have

$$k_c^* = \frac{2}{6 + \frac{\alpha}{\kappa}h_0}\sqrt{\frac{\alpha}{\kappa}\frac{6\Gamma_\perp}{h_0}} \quad \left[\mathrm{m}^{-1}\right] , \tag{44}$$

$$\sigma_M^* = k_c^{*2}\sqrt{\frac{\gamma_s}{\rho}\frac{h_0}{8}} \quad \left[\mathrm{s}^{-1}\right] , \tag{45}$$

where $\Gamma_\perp = \gamma'\Delta_\perp/\gamma_s$. The wavelength of the most amplified mode is

$$\lambda_M^* = \frac{2\sqrt{2}\,\pi}{k_c^*} . \tag{46}$$

We plot in Fig. 11 the wavelength and growth rate of the most amplified modes. We observe that the wavelength increases with the film thickness and that the maximum amplification of perturbations will occur where the thickness is the thinnest, i.e. in the flat film region. Therefore, for a molten silicon film of 100 μm thick, a heat transfer coefficient $\alpha = 1000\ \mathrm{W/(m^2K)}$ and a cross-stream temperature difference $\Delta T_\perp = 1$ K, the wavelength of the Marangoni instability is 1.8 m and the growth rate is about 0.001 s^{-1}. Furthermore, any perturbations of the wavelength smaller than 1.3 m (i.e. $\sim 1.8/\sqrt{2}$) will be stabilized by the system. This result means that a molten silicon sheet that is less than 1.3 m wide will be unconditionally stable. The system becomes more unstable if the heat transfer coefficient α and/or the temperature difference $\Delta T_\perp$ is increased, as shown in Fig. 11.

VII. CONCLUSIONS

We studied the formation of a liquid film pulled out of a bath by means of using thermocapillary stresses prescribed at the free surfaces. The resulting film thickness h_0 essentially depends on the capillary length ℓ_c and on the strength Γ

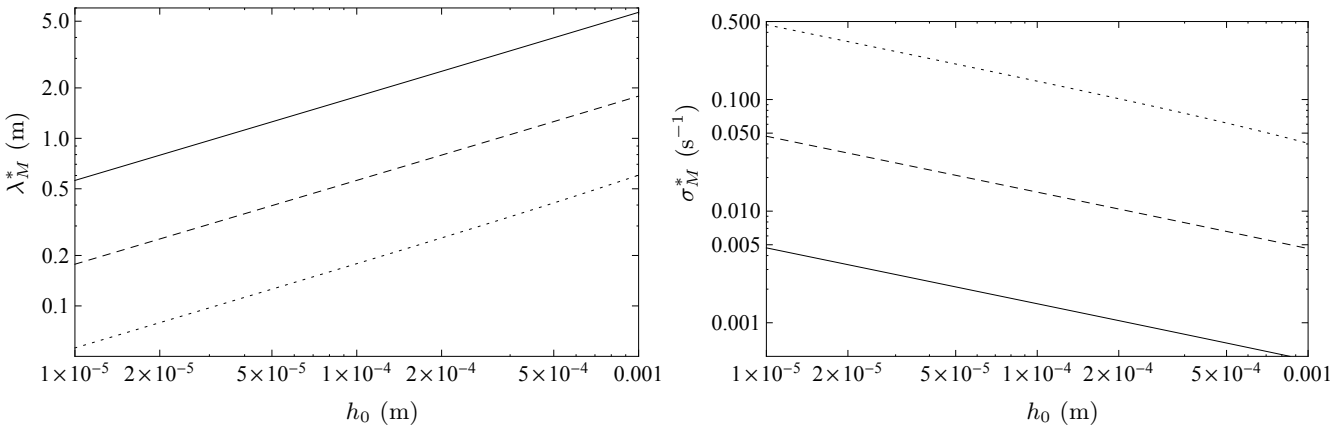

FIG. 11: Wavelength and growth rate of the most amplified mode, versus the thickness h_0 for various heat transfer characteristics: solid line – $\Delta T_\perp = 1$ K and $\alpha = 1000$ W/m^2/K; dashed line – $\Delta T_\perp = 10$ K and $\alpha = 1000$ W/m^2/K; dotted line – $\Delta T_\perp = 10$ K and $\alpha = 10000$ W/m^2/K. The other parameters are taken from Table I.

of the surface tension variation along the interfaces. If the surface tension variation is imposed over a distance d smaller or of the order of the characteristic length of the dynamic meniscus, i.e. $\ell = \sqrt{\ell_c h_0}$ or equivalently $d^* \approx 12\ell_c\sqrt{\Gamma}$, the film thickness is proportional to the temperature difference (or Γ) but is independent of d, as shown by (25). On the contrary, if $d \gg \ell \sim d^*$, the film thickness decreases with the square of the temperature gradient (or Γ/d), as shown by (26). However, gravitational drainage is shown to prevent the formation of a film if $d \gg \ell$, such that this regime corresponds to temperature gradients that are too weak to be relevant for liquid film manufacturing. As a consequence, liquid films can only be formed in the case of strong temperature gradients, i.e. $d \lesssim \ell$, which corresponds for instance to temperature gradient much larger than 1 K/mm for silicon films.

Final film thickness is affected by inertia, regardless the strength of the temperature gradient, and decreases with increasing pulling speed. We also showed that larger heat transfer coefficients, i.e. larger thermocapillary stresses at the interfaces, result in larger thicknesses. Furthermore, if the heat transfer coefficient and/or the pulling speed are not large enough, longitudinal heat conduction can become significant and smooth out the temperature gradient along the interface. We finally address the stability in the transverse direction and show that sufficiently thin films can experience a long-wave Marangoni instability for sufficiently large heat transfer coefficient and/or large temperature difference across the film.

One problem that remains to be analyzed is the longitudinal and transverse stability of the one-dimensional solutions presented in this paper for the dynamic meniscus. Also, the concept of thermocapillary-assisted (high speed) pulling of contact-free films presented in this work relies not only on a very large temperature gradient, i.e. ≈ 100 K/mm, but also on a large effective heat transfer coefficient, i.e. $\alpha > 10^3$ W/(m^{2}K). Although perhaps technologically challenging, such conditions might be approached, among other means, by decreasing the ambient temperature to values that are much below the melting temperature, i.e. $\min(T_a) \ll T_s$, in order to enhance the radiative heat transfer. On the modeling front, this would require solution of the full radiative heat transfer contribution rather than its linearized version, which is valid for $\min(T_a) \sim T_s$. But this configuration also requires accounting for the heat removal at the solidification front as considered for instance by [21] for the edge-defined film-fed growth method. These topics should be the subject of future studies.

Acknowledgments

We thanks the anonymous referees for helpful feedback. B.S. thanks the Brussels Region for funding through the program “Brains Back to Brussels” and acknowledge the support of the “Fonds de la Recherche Scientifique – F.N.R.S”.

Appendix A: Stress balance in the shear-like description

In Eq. (4), we give the relevant stress balance by considering all possible contributions to axial stress, with an implicit assumption of extensional flow. However, as indicated in the text (§III), the final balance of stresses actually leads to a shear-like description of the flow; in fact, this feature is a necessary condition to allow for stable film formation [4]. Here, we demonstrate that an axial stress balance that starts from the implicit assumption of shear flow ends up with the same stress balance as (4), or equivalently (11) in dimensionles form.

We derive below the stress balance equation in the context of the lubrication approximation and with the shear-like distinguished limit for which $Ma = O(\varepsilon^{-1})$ and $Ca = O(\varepsilon^3)$ (see §III). The continuity and the streamwise component of the Navier-Stokes equation in steady-state conditions have the forms

$$\partial_x u + \partial_y v = 0 \,, \tag{A1}$$

$$\rho\left(u\partial_x u + v\partial_y u\right) = -\partial_x p + \eta_s\left(\partial_{xx}u + \partial_{yy}u\right) - \rho g \,, \tag{A2}$$

where the subscripts indicate the derivatives and the viscosity η_s is assumed constant. Following lubrication theory, the pressure is assumed to be uniform in the film cross-section and differs only from the ambient pressure by the Laplace pressure $-\gamma\partial_{xx}(h/2)$. The pressure gradient can then be written as $\partial_x p = -\gamma_s\partial_{xxx}(h/2)$, in which variation of surface tension with temperature has been neglected because $\gamma'\Delta T/\gamma_s \equiv \Gamma \ll 1$ (see Table I). This result would have been obtained by solving the cross-stream component of the Navier-Stokes equation, together with the normal stress balance, which we have by-passed here for the sake of simplicity, but can be found for instance in [9]. The symmetry conditions apply at $y = 0$ (see Fig. 1),

$$\partial_y u = 0 \,, \qquad v = 0 \,, \tag{A3}$$

and the tangential stress condition applies at $y = h/2$:

$$\frac{\eta_s}{n}\left[\left(1 - (\partial_x h)^2\right)(\partial_y u + \partial_x v) - 4\partial_x h\partial_x u\right] = -\gamma'\partial_x T_i \,, \tag{A4}$$

where $n = \sqrt{1 + \frac{1}{4}(\partial_x h)^2}$. The dimensionless variables are

$$X = \frac{x}{\ell}\,, \quad H = \frac{h}{h_0}\,, \quad Y = \frac{y}{h_0}\,,$$
$$U = \frac{u}{u_0}\,, \quad V = \varepsilon\frac{v}{u_0}\,, \quad \Theta_i = \frac{T_i - T_s}{\Delta T}\,,$$

where $H(X)$ is the dimensionless film thickness. The dimensionless equations, truncated at order ε^3 except for the surface tension term, become

$$V_Y = -U_X \,, \tag{A5a}$$

$$U_{YY} = G + \varepsilon Re\left(UU_X + VU_Y\right) - \varepsilon^2 U_{XX} - \frac{\varepsilon^3}{2Ca}H_{XXX} \tag{A5b}$$

$$V = 0 \qquad \text{at } Y = 0 \,, \tag{A5c}$$

$$U_Y = 0 \qquad \text{at } Y = 0 \,, \tag{A5d}$$

$$U_Y = -\varepsilon Ma\Theta_{iX} - \varepsilon^2(4H_X U_X - V_X) \text{ at } Y = \frac{H}{2} \,. \tag{A5e}$$

Assuming $Ca = O(\varepsilon^3)$ and $Ma = O(\varepsilon^{-1})$ as indicated above, as well as $Re = O(1)$ and $G = O(\varepsilon)$, and expanding the variables in powers of ε such as

$$U = U^{(0)} + \varepsilon U^{(1)} \quad \text{and} \quad V = V^{(0)} + \varepsilon V^{(1)} \,, \tag{A6}$$

the system of equations at leading order in ε has the form

$$V_Y^{(0)} = -U_X^{(0)} \,, \tag{A7a}$$

$$U_{YY}^{(0)} = -\frac{\varepsilon^3}{2Ca}H_{XXX} \,, \tag{A7b}$$

$$V^{(0)} = 0 \qquad \text{at } Y = 0 \,, \tag{A7c}$$

$$U_Y^{(0)} = 0 \qquad \text{at } Y = 0 \,, \tag{A7d}$$

$$U_Y^{(0)} = -\varepsilon Ma \Theta_{iX} \qquad \text{at } Y = \frac{H}{2} \,. \tag{A7e}$$

Integrating (A7b) twice with respect to Y, using (A7d) as well as mass conservation

$$2\int_0^{H/2} U^{(0)} \, \mathrm{d}Y = 1 \,, \tag{A8}$$

gives the leading-order streamwise velocity profile

$$U^{(0)}(X,Y) = \frac{1}{H} + \frac{\varepsilon^3}{2Ca} H_{XXX} \left(\frac{H^2}{24} - \frac{Y^2}{2} \right) \,. \tag{A9}$$

Inserting (A9) into (A7e) yields the leading-order longitudinal stress balance

$$2\varepsilon Ma \Theta_{iX} - \frac{\varepsilon^3}{2Ca} H H_{XXX} = 0 \,. \tag{A10}$$

To proceed to next order in the ε expansion, we first need to determine the leading-order transverse velocity field by integrating (A7a) with (A7c),

$$\begin{aligned} V^{(0)} &= \frac{H_X}{H^2} Y - \frac{\varepsilon^3}{48Ca} Y \left[2H H_X H_{XXX} \right. \\ &+ \left. (H^2 - 4Y^2) H_{XXXX} \right] \,. \end{aligned} \tag{A11}$$

The problem to be solved at first-order is

$$U_{YY}^{(1)} = \varepsilon Re \left(U^{(0)} U_X^{(0)} + V^{(0)} U_Y^{(0)} \right) + G \,, \tag{A12a}$$

$$U_Y^{(1)} = 0 \qquad \text{at } Y = 0 \,, \tag{A12b}$$

which can be integrated twice with respect to Y, while ensuring mass conservation with

$$\int_0^{H/2} U^{(1)} \, \mathrm{d}Y = 0 \,. \tag{A13}$$

The first-order correction to the velocity profile is thus obtained as

$$U^{(1)} = \left(\frac{Re H_X}{H^3} - G \right) \left(\frac{H^2}{24} - \frac{Y^2}{2} \right) + O(\varepsilon^3) \,. \tag{A14}$$

Substituting $U = U^{(0)} + \varepsilon U^{(1)}$ into (A5e) truncated at first order leads finally to

$$2\varepsilon Ma \Theta_{iX} - \frac{\varepsilon^3}{2Ca} H H_{XXX} + GH - \varepsilon Re \frac{H_X}{H^2} = 0 \,, \tag{A15}$$

which is identical to (11) without the extensional viscous term that is an ε^2-order term in the asymptotic expansion. Note also that the one-dimensional assumption for the temperature field implies that $\Theta_i = \bar{\Theta}(X)$. This assumption is discussed in Appendix B.

Appendix B: One-dimensional temperature equation

In this appendix, we demonstrate how the one-dimensional equation for the temperature field is derived and how it can be corrected to account for a temperature variation across the film induced by interfacial heat transfer. The steady-state energy equation has the form

$$\rho c_p \left(u \partial_x T + v \partial_y T \right) = \kappa \left(\partial_{yy} T + \partial_{xx} T \right) \,, \tag{B1}$$

where c_p is the specific heat capacity and κ is the thermal conductivity. The symmetry condition applies at $y = 0$,

$$\partial_y T = 0 \,, \tag{B2}$$

and Newton's cooling law applies at the interface $y = h/2$,

$$\kappa \partial_y T = -\alpha \left(T - T_a(x) \right) \,, \tag{B3}$$

where a small slope, i.e. $|\partial_x h| \ll 1$, has been assumed for simplicity [22]. Using the same scaling as before, the dimensionless equations for the temperature become

$$\Theta_{YY} = \varepsilon Pe \left(U \Theta_X + V \Theta_Y \right) - \varepsilon^2 \Theta_{XX} \,, \tag{B4a}$$

$$\Theta_Y = -Bi(\Theta - \Theta_a) \qquad \text{at} \quad Y = \frac{H(X)}{2} \,, \tag{B4b}$$

$$\Theta_Y = 0 \qquad \text{at} \quad Y = 0 \,, \tag{B4c}$$

where the Péclet and Biot numbers are defined as

$$Pe = \frac{\rho c_p u_0 h_0}{\kappa} \quad \text{and} \quad Bi = \frac{\alpha h_0}{\kappa} \,,$$

and $\varepsilon = h_0/\ell$ is the slenderness parameter. Even though we consider $St = 2Bi/(\varepsilon Pe) \gtrsim 1$, the way the one-dimensional temperature equation is obtained will differ slightly depending on the magnitude of the heat advected by the flow, transferred to the surrounding and conducted along the film, as discussed next.

1. Small heat transfer: $Bi = O(\varepsilon)$ and $Pe = O(1)$

In the case of small heat transfer from the film to the surroundings, by expanding the temperature field as $\Theta(X, Y) = \Theta^{(0)} + \varepsilon \Theta^{(1)} + \varepsilon^2 \Theta^{(2)}$, the system of equations (B4a-B4c) at leading order becomes

$$\Theta^{(0)}_{YY} = 0 \,, \tag{B5a}$$

$$\Theta^{(0)}_{Y} = 0 \qquad \text{at} \quad Y = \frac{H}{2} \,, \tag{B5b}$$

$$\Theta^{(0)}_{Y} = 0 \qquad \text{at} \quad Y = 0 \,. \tag{B5c}$$

The solution is simply a uniform temperature profile across the film $\Theta^{(0)} = \bar{\Theta}(X)$. At first order, the system becomes

$$\Theta^{(1)}_{YY} = \varepsilon Pe U^{(0)} \bar{\Theta}_X \,, \tag{B6a}$$

$$\Theta^{(1)}_{Y} = -Bi(\bar{\Theta} - \Theta_a) \qquad \text{at} \quad Y = \frac{H}{2} \,, \tag{B6b}$$

$$\Theta^{(1)}_{Y} = 0 \qquad \text{at} \quad Y = 0 \,, \tag{B6c}$$

which can be integrated across the thickness using (A9) and (A11) to yield

$$\bar{\Theta}_X = -St \left(\bar{\Theta} - \Theta_a \right) \,, \tag{B7}$$

with $St = 2Bi/(\varepsilon Pe)$. This equation is identical to (14).

2. Large heat transfer: $Bi = 1$ and $Pe = O(1/\varepsilon)$

In the case of large heat transfer from the liquid to the surroundings, the temperature profile across the film cannot be uniform anymore at leading order. One can for instance assume a parabolic profile that satisfies the boundary conditions (B4b) and (B4c), and is written in terms of the average temperature $\bar{\Theta} = (2/H) \int_0^{H/2} \Theta \, \mathrm{d}Y$:

$$\Theta(X, Y) = \Theta_a + \left(\frac{\bar{\Theta} - \Theta_a}{1 + \frac{Bi}{6} H} \right) \left(1 + BiH \left(\frac{1}{4} - \frac{Y^2}{H^2} \right) \right) \,. \tag{B8}$$

Inserting (B8), (A9) and (A11) into (B4a) yields

$$\bar{\Theta}_X = -St\frac{(\bar{\Theta} - \Theta_a)}{1 + \frac{Bi}{6}H} \ , \tag{B9}$$

where the higher-order terms in (A9,A11) have been neglected. We note that the only difference between (B9) and (B7) is the denominator of the right-hand side that accounts for the parabolic temperature profile across the film. This equation has been used for instance in [17] to model the heat transfer in stretching glass sheets, where it has been shown that a non-uniform temperature profile across the film does not qualitatively change the film profile as compared to the case of a uniform temperature profile.

3. Diffusive case: $Bi = O(\varepsilon^2)$ and $Pe = O(\varepsilon)$

We finally consider the case $Pe = O(\varepsilon)$ corresponding to large heat conduction or equivalently small pulling speeds. Because conduction terms are of order ε^2, one should set $Bi = O(\varepsilon^2)$ to have diffusive and interfacial transfer effects at the same order. Expanding then (B6a) up to second-order gives

$$\Theta^{(2)}_{YY} = \varepsilon Pe U^{(0)}\bar{\Theta}_X - \varepsilon^2\bar{\Theta}_{XX} \ . \tag{B10a}$$

$$\Theta^{(2)}_{Y} = -Bi(\bar{\Theta} - \Theta_a) \qquad \text{at} \quad Y = \frac{H}{2} \ , \tag{B10b}$$

$$\Theta^{(2)}_{Y} = 0 \qquad \text{at} \quad Y = 0 \ . \tag{B10c}$$

Integrating (B10a) using (B10b) and (B10c) yields

$$\bar{\Theta}_X = -St\left(\bar{\Theta} - \Theta_a\right) + \frac{\varepsilon}{Pe}\bar{\Theta}_{XX} \ , \tag{B11}$$

which is identical to (30).

Appendix C: Linearization of radiative heat transfer

The stationary version of the one-dimensional temperature equation with pure radiative heat transfer has the form

$$\rho c_p h\bar{u}\bar{T}_x = -2\varepsilon_T\sigma_{\rm SB}\left(\bar{T}^4 - T_a^4\right) \ , \tag{C1}$$

where ε_T is the total emissivity of the molten liquid and $\sigma_{\rm SB}$ is the Stefan-Boltzmann constant. In dimensionless form, using the scales introduced in §II C, (C1) becomes

$$\bar{\Theta}_X = -\frac{St}{4\tau}\left[\left(1 + \tau\bar{\Theta}\right)^4 - \left(1 + \tau\Theta_a\right)^4\right] \ , \tag{C2}$$

where $\tau = \Delta T/T_s$ and St is constructed with $\alpha \equiv \alpha_R = 4\varepsilon_T\sigma_{\rm SB}T_s^3$. Since $\Delta T/T_s \ll 1$ (see Table I), (C2) can be linearized around τ, which leads back to the convective heat transfer equation (14) that is used throughout this paper. The corresponding radiative heat transfer coefficient can be evaluated by taking $\varepsilon_T = 0.3$ for the total emissivity of liquid silicon [23] and with $\sigma_{\rm SB} = 5.67 \times 10^{-8}$ W/(m^{2}K^4), which gives $\alpha_R = 327$ W/(m^{2}K).

[1] D. Helmreich and E. Sirtl, "Progress in ingot and foil casting of silicon," J. Cryst. Growth, **79**, 562–571 (1986).
[2] A. G. Schoenecker and K. I. Steinbach, "Method and device for producing metal foils," Patent EP1743385(B1) (2008).
[3] J. D. Zook and S. B. Schuldt, "Analysis of conditions for high-speed growth of silicon sheet," J. Cryst. Growth, **50**, 51–61 (1980).
[4] E. A. van Nierop, B. Scheid, and H. A. Stone, "On the thickness of soap films: An alternative to frankel's law," J. Fluid Mech., **602**, 119–127 (2008), Corrigendum: **630**, 443 (2009).
[5] K. J. Mysels, K. Shinoda, and S. Frankel, *Soap Films: Studies of Their Thinning* (Pergamon, London, 1959).
[6] B. Scheid, E. van Nierop, and H. A. Stone, "Thermocapillary-assisted pulling of thin films: Application to molten metals," Appl. Phys. Lett., **97**, 171906 (2010).

[7] Z. Zhou, S. Mukherjee, and A.-K. Rhim, "Measurement of thermophysical properties of molten silicon using an upgraded electrostatic levitator," J. Cryst. Growth, **257**, 350–358 (2003).

[8] The thermal expansion coefficient is usually small for typical liquids (its value is 7×10^{-5} K^{-1} for silicon at the melting temperature [7]). Buoyancy effect can thus be safely neglected given the smallness of our system dimensions, meaning that the Rayleigh number remains much smaller than its critical value, even if constructed with the largest length-scale of the system.

[9] C. J. Breward, *The Mathematics of Foam*, PhD thesis, Oxford University (1999).

[10] F. Cao, R. E. Khayat, and J. E. Puskas, "Effect of inertia and gravity on the draw resonance in high-speed film casting of newtonian fluids," Intl J. Solids Struct., **42**, 5734–5757 (2005).

[11] S. Smith and D. Stolle, "Nonisothermal two-dimensional film casting of a viscous polymer," Polym. Eng. Sc., **40**, 1870 (2000).

[12] C. J. Breward and P. D. Howell, "The drainage of a foam lamella," J. Fluid Mech., **458**, 379–406 (2002).

[13] P.-G. de Gennes, F. Brochart-Wyart, and D. Quéré, *Gouttes, Bulles, Perles et Ondes* (Belin (Paris), 2005).

[14] L. Landau and B. Levich, "Dragging of a liquid by a moving plate," Acta Physicochim. URSS, **17**, 42 (1942).

[15] B. V. Derjaguin, Acta Physicochim. URSS, **20**, 349 (1943).

[16] For liquids that experience a glass transition however, because of the exponential increase of the viscosity in the x direction due to cooling, there might be a location where Υ becomes equal or larger than ε^{-2}. This case would correspond to an intermediate regime in which capillary, Marangoni and extensional viscous forces all balance. Such an analysis is beyond the scope of the present work.

[17] B. Scheid, S. Quiligotti, B. Tran, R. Gy, and H. A. Stone, "On the (de)stabilization of draw resonance due to cooling," J. Fluid Mech., **636**, 155 (2009).

[18] P. Carles and A. Cazabat, "The thickness of surface-tension-gradient-driven spreading flims," J. Colloid Interface Sci., **157**, 196–201 (1993).

[19] P. Carles, A. Cazabat, and E. Kolb, "The spreading of films by surface tension gradients," Colloids Surf. A, **79**, 65–70 (1993).

[20] A. de Ryck and D. Quéré, "Gravity and inertia effects in plate coating," J. Colloid Interface Sci., **203**, 278–285 (1998).

[21] P. Thomas, H. Ettouney, and R. Brown, "A thermal-capillary mechanism for a growth rate limit in edge-defined film-fed growth of silicon sheets," J. Cryst. Growth, **76**, 339 (1986).

[22] The small slope assumption is inherent to the lubrication approximation since $|\partial_x h| \sim \varepsilon$. The higher order terms arising from surface deformability, formally of order ε^2, have thus been neglected in (B3) as they disappear from the asymptotic expansion performed in what follows.

[23] M. Lampert, J. Koebel, and P. Siffert, "Temperature dependence of the reflectance of solid and liquid silicon," J. Appl. Phys., **52**, 4975 (1981).